

Modeling and Optimal Operation of Distributed Battery Storage in Low Voltage Grids

Philipp Fortenbacher, Johanna L. Mathieu, and Göran Andersson

Abstract—Due to high power in-feed from photovoltaics, it can be expected that more battery systems will be installed in the distribution grid in near future to mitigate voltage violations and thermal line and transformer overloading. In this paper, we present a two-stage centralized model predictive control scheme for distributed battery storage that consists of a scheduling entity and a real-time control entity. To guarantee secure grid operation, we solve a robust multi-period optimal power flow (OPF) for the scheduling stage that minimizes battery degradation and maximizes photovoltaic utilization subject to grid constraints. The real-time controller solves a real-time OPF taking into account storage allocation profiles from the scheduler, a detailed battery model, and real-time measurements. To reduce the computational complexity of the controllers, we present a linearized OPF that approximates the nonlinear AC-OPF into a linear programming problem. Through a case study, we show, for two different battery technologies, that we can substantially reduce battery degradation when we incorporate a battery degradation model. A further finding is that we can reduce battery losses by 30% by using the detailed battery model in the real-time control stage.

Index Terms—optimal control, power systems, predictive control, energy storage

I. INTRODUCTION

IN the next few years, it can be expected that many battery systems will be installed in the Low Voltage (LV) distribution grid to cope with high in-feed from photovoltaics (PV) [1] and other fluctuating energy sources also connected to the distribution grid. In particular, battery systems can mitigate voltage violations and thermal line overloading, allowing Distribution System Operators (DSOs) to defer line and transformer upgrades. Some recent papers [2], [3] developed decentralized battery control strategies to provide voltage support. Decentralized control strategies have the advantage that they rely only on local measurements. Thus, they do not require communication infrastructure. However, addressing thermal overloading requires coordination either via centralized or distributed control, since the power flows are not observable at a local level. In [4], a centralized predictive control scheme is developed to avoid thermal line overloading, but the authors do not consider voltage constraints. Furthermore, the proposed control strategies in [2], [3], [4] do not consider battery degradation or use detailed battery models.

Since investment costs for batteries are still high [5], a battery's expected lifetime greatly affects assessments of its

economic viability. Each control action applied to a battery leads to charge capacity loss (i.e., degradation) [6], reducing its lifetime. Some recent papers propose methods to include battery degradation costs in economic cost functions [7], [8]. Another way to increase the economic viability of a battery is to exploit its full capacity, enabling operation in low/high state of charge regimes when the benefits outweigh the degradation costs. However, simple battery models do not capture the dynamics that are present when batteries operate in these regimes. For example, operation in these regimes is only possible at low charging/ discharging powers. It is possible to model these dynamics with detailed battery models [9], [10].

The objective of this paper is to develop computationally-tractable methods to control distributed batteries in distribution networks with high penetrations of PV to manage network constraints such as voltage and thermal constraints. To exploit the full potential of the network and to dispatch the battery systems in an economic and efficient way, we formulate multi-period AC Optimal Power Flow (AC-OPF) problems. We use a linear approximation of the AC-OPF from our previous work [11] that exploits the radial structure of a LV network. While convex relaxations of the nonlinear nonconvex AC-OPF problem exist, the resulting semi definite [12] and second order cone [13], [14] programs are computationally large and not suitable for computationally-limited controllers. Our contribution is to incorporate this linear AC-OPF into a two-stage Model Predictive Control (MPC) control scheme that consists of a scheduler and a real-time (RT) controller. The scheduler is a robust MPC that solves a multi-period Optimal Power Flow (OPF) minimizing battery degradation and maximizing PV utilization subject to grid and storage constraints. We link the planning domain with the RT domain by computing storage allocation bounds that are used by the RT controller, which solves an RT-OPF using a detailed battery model and RT measurements of the network and battery states to minimize the battery and network losses.

This paper is organized as follows: Section II defines the problem that we aim to solve. Section III presents the battery models used in the proposed controllers. Section IV reviews the linearized OPF formulation that is included in our controllers. Section V describes the controller formulations for the scheduler and RT controller. Section VI presents the simulation results and a battery lifetime assessment. Finally, Section VII presents the conclusions.

II. PROBLEM DEFINITION

Existing inverter-level strategies to maximize PV infeed include active power curtailment [15] and reactive power

This work was in part financed by the Swiss Commission of Technology and Innovation (CTI).

P. Fortenbacher and G. Andersson are with the Power Systems Laboratory, ETH Zurich, Switzerland. (e-mail: fortenbacher@eeh.ee.ethz.ch, andersson@eeh.ee.ethz.ch)

J. L. Mathieu is with the Department of Electrical and Computer Engineering, University of Michigan, USA. (e-mail: jlmath@umich.edu)

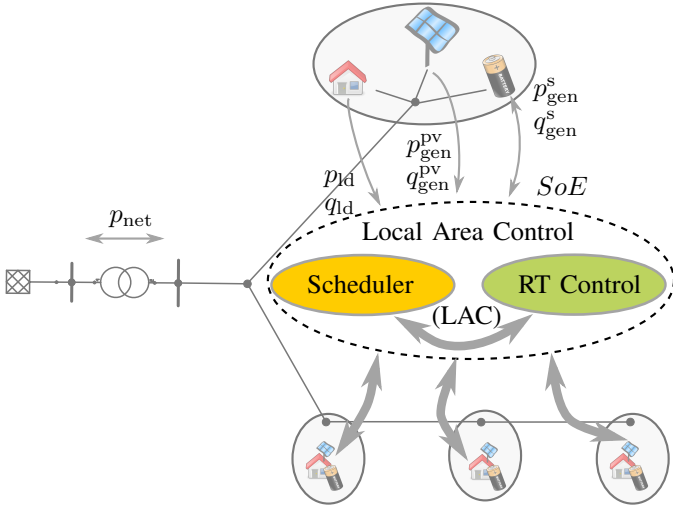


Figure 1. Illustration of the problem environment. The overall control objective is to maximize PV infeed while managing grid constraints and minimizing battery degradation.

control [16], which are used by DSOs in Germany [17]. In contrast to OPF methods, no communication infrastructure is needed. However, OPF methods enable optimal utilization of the grid. We propose a method that combines distribution-level OPF with a storage control strategy that could leverage high bandwidth communication links already available at most households.

Figure 1 illustrates the problem environment. Battery systems are used to mitigate voltage violations and thermal line overloading that results from high PV infeed in LV networks, enabling the DSO to defer equipment upgrades. The overall control objective is to maximize PV infeed, while managing grid constraints and minimizing battery degradation. PV maximization can be achieved by minimizing the net power p_{net} . We assume a local area control (LAC) entity that computes an optimal allocation schedule for the storage devices every hour for a 24 hours horizon. It uses the storage allocation schedule, knowledge of each battery's state of energy (SOE), and RT measurements of the active and reactive power consumption of the loads (p_{ld} , q_{ld}) and power production of the PV generators (p_{gen}^{pv} , q_{gen}^{pv}) to solve an RT-OPF to compute RT active and reactive power battery setpoints (p_{gen}^s , q_{gen}^s) every 10 seconds.

III. BATTERY MODELING

In this section, we extend the linear battery models developed in our previous work [9]. The resulting models capture the main relevant characteristics of battery systems and allow for tractable controller formulations.

A. Efficiency

In order to determine the cost optimal operation of multiple battery systems, we first need a model that describes the total efficiency of an individual battery system considering both the battery and inverter losses. The models developed in [9] only included the battery losses so we extend them to include the inverter losses. Figure 2 shows a block diagram

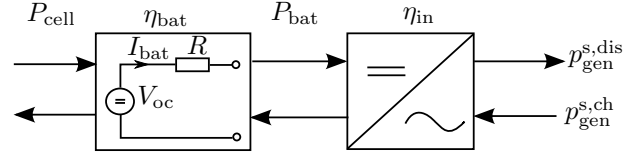


Figure 2. Block diagram of a battery system consisting of a grid connected inverter (right block) and battery stack (left block).

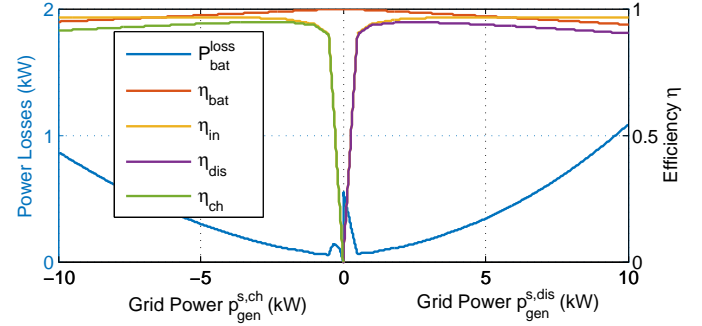


Figure 3. Battery system efficiencies and total power losses as a function of the grid power. The plot is calculated for a 10kW battery system with $R=10\text{m}\Omega$, $V_{oc}=42\text{V}$, and a standard inverter efficiency curve from [18].

of a battery system. The crucial parameter that influences the battery efficiency η_{bat} is the battery's internal resistance R . Using a Thevenin circuit equivalent, the battery power P_{bat} is

$$P_{bat} = V_{oc}I_{bat} - RI_{bat}^2, \quad (1)$$

where V_{oc} is the open circuit voltage (OCV). The battery efficiency for discharging currents $I_{bat} > 0$ is

$$\eta_{bat}^{dis} = \frac{P_{bat}}{P_{cell}} = \frac{V_{oc}I_{bat} - RI_{bat}^2}{V_{oc}I_{bat}} = 1 - \frac{RI_{bat}}{V_{oc}}, \quad (2)$$

where the internal cell power P_{cell} is referred to as the power input. The battery efficiency for charging currents $I_{bat} < 0$ is

$$\eta_{bat}^{ch} = \frac{P_{cell}}{P_{bat}} = 1 + \frac{RI_{bat}}{V_{oc} - RI_{bat}}. \quad (3)$$

For $V_{oc} \gg RI_{bat}$, we can approximate η_{bat}^{ch} as follows:

$$\eta_{bat}^{ch} \approx \eta_{bat}^{dis} = 1 - \left| \frac{RI_{bat}}{V_{oc}} \right|. \quad (4)$$

The battery efficiency can be expressed as a function of P_{bat} by solving (1) for I_{bat} and substituting the resulting expression into (4)

$$\eta_{bat} = 1 - \left| \frac{V_{oc} - \sqrt{V_{oc}^2 - 4RP_{bat}}}{2V_{oc}} \right|. \quad (5)$$

Including the inverter efficiency η_{in} the total losses are

$$P_{loss}^{bat} = \begin{cases} (\eta_{bat}^{-1}\eta_{in}^{-1} - 1)p_{gen}^{s,dis} = (\eta_{dis}^{-1} - 1)p_{gen}^{s,dis} \\ (\eta_{bat}\eta_{in} - 1)p_{gen}^{s,ch} = (\eta_{ch} - 1)p_{gen}^{s,ch}, \end{cases} \quad (6)$$

where $p_{gen}^{s,dis} \geq 0$ and $p_{gen}^{s,ch} < 0$ represent the discharging and charging grid powers. The multiplication of η_{bat} and η_{in} leads to a non-convex loss function, which is shown in Fig. 3 (blue curve). The inverter efficiency is obtained from [18].

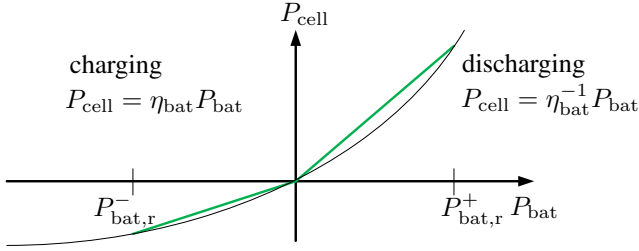


Figure 4. Linear approximation of the cell power P_{cell} with respect to the battery power P_{bat} .

B. Dynamics

We also model fast battery dynamics. The models in [9] expressed the state variable in terms of charge, and here we express it in terms of energy for convenience.

1) *Linear Basic Model*: The first model is an integrator model

$$S\dot{o}E = -P_{\text{cell}} \quad , \quad (7)$$

where SoE denotes the time-varying state of energy. As shown in Fig. 4, P_{cell} is a nonlinear function of the battery power. To derive a linear model, we linearize P_{cell} between 0 and rated powers $P_{\text{bat},r}^-$, $P_{\text{bat},r}^+$ by evaluating (5) at those points. By including an averaged inverter efficiency $\bar{\eta}_{\text{in}}$, we obtain

$$S\dot{o}E \approx \underbrace{\begin{bmatrix} -\eta_{\text{bat}}(P_{\text{bat},r}^+)^{-1}\bar{\eta}_{\text{in}}^{-1} & -\eta_{\text{bat}}(P_{\text{bat},r}^-)\bar{\eta}_{\text{in}} \end{bmatrix}}_{\mathbf{b}_{\text{bat}}^T} \begin{bmatrix} p_{\text{gen}}^{\text{s,dis}} \\ p_{\text{gen}}^{\text{s,ch}} \end{bmatrix}. \quad (8)$$

2) *Linear Extended Model*: The linear extended model allows us to capture the rate capacity effect [19]. This effect accounts for the ion diffusion in the electrolyte and reduces the accessible battery capacity for high battery powers. As we have presented in [9] we capture this effect by modifying the KiBaM model [20]. The model is

$$\dot{\mathbf{x}}_E = \underbrace{\begin{bmatrix} -\frac{c_r}{c_w} & \frac{c_r}{1-c_w} \\ \frac{c_r}{c_w} & -\frac{c_r}{1-c_w} \end{bmatrix}}_{\mathbf{A}} \mathbf{x}_E + \begin{bmatrix} \mathbf{b}_{\text{bat}}^T \\ \mathbf{0} \end{bmatrix} \begin{bmatrix} p_{\text{gen}}^{\text{s,dis}} \\ p_{\text{gen}}^{\text{s,ch}} \end{bmatrix} \quad (9)$$

$$SoE = x_{E1} + x_{E2} \quad ,$$

where $\mathbf{x}_E = [x_{E1}, x_{E2}]^T$ denotes the state vector for two virtual wells that are interconnected. Energy can only be withdrawn from the available well x_{E1} . The parameter c_w determines the size of the wells and c_r is the inverse charge recovery time.

C. Degradation

Charge capacity loss in lithium ion (Li-ion) batteries is a slow process and hard to model. Among the contributors to capacity loss are two chemical side reactions that irreversibly transform cyclable ions into solids during battery operation. In [9], we presented a method to identify a stationary degradation process on an arbitrary battery usage pattern. The method produces a degradation map, where degradation is a function of the battery power and state of energy. Unfortunately,

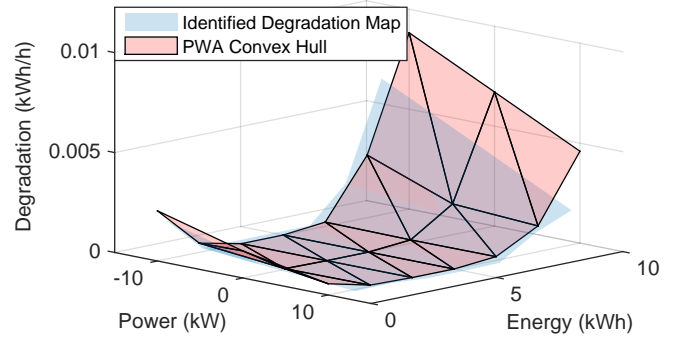


Figure 5. Illustration of the degradation map for a 10 kWh battery system ($c_E = 10\text{kWh}$). The red surface is the piecewise affine (PWA) convex hull (10) of the identified map (blue surface).

degradation maps are in general nonconvex [21], such that we cannot apply efficient convex solvers in our optimization framework. As an extension to the work in [9], we compute the convex hull of the degradation map from [9] using Delaunay triangulation [22]. Figure 5 shows the convex hull (red surface) of the identified degradation map (blue surface). By evaluating the plane parameters $\mathbf{a}_1, \mathbf{a}_2, \mathbf{a}_3$ of the triangles from the convex hull, we can define the following piecewise affine mapping for the degradation z :

$$z = \max \left([\mathbf{a}_1 \ \mathbf{a}_2] \begin{bmatrix} P_{\text{bat}} \\ SoE \end{bmatrix} + \mathbf{a}_3 c_E \right) \quad , \quad (10)$$

where c_E is the battery energy capacity.

IV. OPTIMAL POWER FLOW FOR LOW VOLTAGE GRIDS

In our previous work [10], [11], we derived a linearized OPF formulation. Based on the Forward Backward Sweep (FBS) power flow method from [23], we linearly approximated voltage, power losses, and branch flow limits as linear functions of the nodal reactive and active power injections. The following assumptions were made.

- We assume three-phase balanced radial LV networks. Three-phase balanced LV networks are common in Europe [24]; however, this assumption is less valid for the U.S., but in principle the proposed OPF method could also be extended for unbalanced networks [23].
- We assume that LV networks have high resistance over reactance ratios ($R/X \geq 2$) [24].
- We assume that voltage angle differences in LV networks are small ($\leq 10^\circ$).

We summarize the formulation here; for full details see [11].

First, we give the generic formulation, before we specialize it to our scenario in Section V. We define following decision vector $\mathbf{x} = [p_{\text{gen}}, q_{\text{gen}}, \mathbf{p}_1^p, \mathbf{p}_1^q, \mathbf{v}]^T$, where $p_{\text{gen}} \in \mathbb{R}^{n_g \times 1}$ and $q_{\text{gen}} \in \mathbb{R}^{n_g \times 1}$ are the active and reactive generator powers, where n_g is the number of generators; $\mathbf{p}_1^p \in \mathbb{R}^{n_l \times 1}$ and $\mathbf{p}_1^q \in \mathbb{R}^{n_l \times 1}$ are the approximate active power losses due to active and reactive power injections (defined in [11]), where n_l is the number of lines; and $\mathbf{v} \in \mathbb{R}^{n \times 1}$ is the voltage vector, where n is the number of buses. Assuming positive linear costs c_p for the active generator powers, the OPF problem

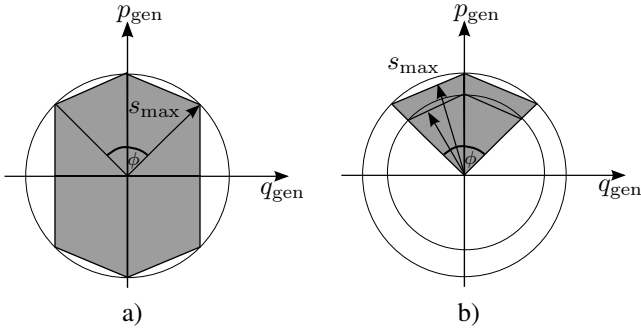


Figure 6. Approximated reactive power capability areas a) circular-bounded b) $\cos \phi$ -bounded. The polygonal convex regions can be described with the constraints (11h-l). [10]

can be approximated as the following Linear Programming (LP) problem:

$$\begin{aligned}
 J^* &= \min_x \mathbf{c}_p^T \mathbf{p}_{\text{gen}} \\
 \text{s.t. } & \text{(a) } \mathbf{1}^T \mathbf{C}_g \mathbf{p}_{\text{gen}} - \mathbf{1}^T \mathbf{p}_1^p - \mathbf{1}^T \mathbf{p}_1^q = \mathbf{1}^T \mathbf{p}_d \\
 & \text{(b) } \mathbf{B}_v \begin{bmatrix} \mathbf{C}_g \mathbf{p}_{\text{gen}} \\ \mathbf{C}_g \mathbf{q}_{\text{gen}} \end{bmatrix} - \mathbf{v} = \mathbf{B}_v \begin{bmatrix} \mathbf{p}_d \\ \mathbf{q}_d \end{bmatrix} - \mathbf{v}_s \\
 & \text{(c) } \mathbf{B}_1^1 \mathbf{p}_1^p - \mathbf{B}_1^2 \mathbf{C}_g \mathbf{p}_{\text{gen}} \geq \mathbf{B}_1^2 \mathbf{p}_d + \mathbf{b}_1 \\
 & \text{(d) } \mathbf{B}_1^1 \mathbf{p}_1^q - \mathbf{B}_1^2 \mathbf{C}_g \mathbf{q}_{\text{gen}} \geq \mathbf{B}_1^2 \mathbf{q}_d + \mathbf{b}_1 \\
 & \text{(e) } -i_b^{\max} + \mathbf{B}_r \mathbf{p}_d \leq \mathbf{B}_r \mathbf{C}_g \mathbf{p}_{\text{gen}} \leq i_b^{\max} + \mathbf{B}_r \mathbf{p}_d \\
 & \text{(f) } \mathbf{v}_{\min} \leq \mathbf{v} \leq \mathbf{v}_{\max} \\
 & \text{(g) } \mathbf{p}_{\min} \leq \mathbf{p}_{\text{gen}} \leq \mathbf{p}_{\max} \\
 & \text{(h) } \mathbf{p}_{\text{gen}} + \mathbf{A}_q \mathbf{q}_{\text{gen}} \leq \mathbf{s}_{\max} \\
 & \text{(i) } \mathbf{p}_{\text{gen}} - \mathbf{A}_q \mathbf{q}_{\text{gen}} \leq \mathbf{s}_{\max} \\
 & \text{(j) } \mathbf{p}_{\text{gen}} + \mathbf{A}_q \mathbf{q}_{\text{gen}} \geq -\mathbf{s}_{\max} \\
 & \text{(k) } \mathbf{p}_{\text{gen}} - \mathbf{A}_q \mathbf{q}_{\text{gen}} \geq -\mathbf{s}_{\max} \\
 & \text{(l) } -\mathbf{B}_q \mathbf{s}_{\max} \leq \mathbf{q}_{\text{gen}} \leq \mathbf{B}_q \mathbf{s}_{\max} \quad ,
 \end{aligned} \tag{11}$$

where $\mathbf{p}_d \in \mathbb{R}^{n \times 1}$ and $\mathbf{q}_d \in \mathbb{R}^{n \times 1}$ are the active and reactive net load; $\mathbf{C}_g \in \mathbb{R}^{n \times n_g}$ maps generators to buses; and \mathbf{B}_v , \mathbf{B}_r , \mathbf{A}_q , and \mathbf{B}_q are matrix parameters defined in [11] and [10]. Constraint (11a) enforces power balance in the grid. The voltage approximation is included in (11b), where each element of $\mathbf{v}_s \in \mathbb{R}^{n_1 \times 1}$ is the slack bus voltage. The constraints (11c,d) incorporate epigraph formulations that are piecewise linear inner approximations of the power losses. We specify the matrix and vector parameters \mathbf{B}_1^1 , \mathbf{B}_1^2 , and \mathbf{b}_1 to obtain a more compact form of the inequalities defined in [11]. Note that to get an optimal solution the solver can only select values that lie on the defined hyperplanes. Constraint (11e) includes branch flow limits, where $i_b \in \mathbb{R}^{n_1 \times 1}$ are the branch flow currents. Constraints (11f,g) specify the lower and upper bounds for the voltage (\mathbf{v}_{\min} , \mathbf{v}_{\max}) and active generator powers (\mathbf{p}_{\min} , \mathbf{p}_{\max}). Constraints (11h-l) approximate the generators' apparent power limits, where \mathbf{s}_{\max} is the generators' maximum apparent power; specifically, we define circular-bounded and $\cos \phi$ -bounded active and reactive power settings by approximating the circular area/segments with convex sets [10] that describe the polygons depicted in Fig 6.

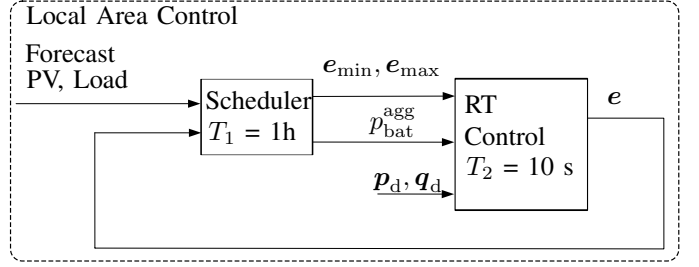


Figure 7. Centralized control scheme consisting of a scheduler and an RT controller. The scheduler uses robust MPC. The RT controller solves a RT-OPF using the storage allocation from the scheduler and RT measurements.

V. OPTIMAL BATTERY OPERATION

A. Control Structure

As shown in Fig. 7 our proposed control scheme consists of two control entities working at different time scales. We do not allow for PV curtailment and so the scheduler has to calculate future storage allocation bounds in terms of energy e_{\min} , e_{\max} and aggregated power $p_{\text{bat}}^{\text{agg}}$ that are feasible under the worst case PV forecast scenarios. The RT controller tries to control the storage units within these bounds, while minimizing network and storage losses and taking into account RT measurements of the net load.

B. Scheduler

We solve a robust multi-period OPF subject to the worst case PV predictions. Since we solve the multi-period problems in a receding horizon fashion every hour with updated energy levels, the scheduler acts as a robust MPC.

1) *Incorporation of Distributed Storage:* Due to its low sample time $T_1 = 1$ hour, the scheduler cannot capture the detailed battery dynamics so we use the linear basic model (8). The discrete version of (8) for n_s battery systems is

$$\mathbf{e}(k+1) = \mathbf{I}^{n_s} \mathbf{e}(k) + \underbrace{T_1 \begin{bmatrix} \text{diag}\{-\eta_{\text{dis}}^{-1}\} & \text{diag}\{-\eta_{\text{ch}}\} \end{bmatrix}}_{\mathbf{B}} \underbrace{\begin{bmatrix} \mathbf{p}_{\text{gen}}^{\text{s,dis}} \\ \mathbf{p}_{\text{gen}}^{\text{s,ch}} \end{bmatrix}}_{\mathbf{p}_{\text{gen}}^{\text{s}}}, \tag{12}$$

where $\mathbf{p}_{\text{gen}}^{\text{s,dis}} \geq \mathbf{0} \in \mathbb{R}^{n_s \times 1}$, $\mathbf{p}_{\text{gen}}^{\text{s,ch}} < \mathbf{0} \in \mathbb{R}^{n_s \times 1}$, $\eta_{\text{dis}}, \eta_{\text{ch}} \in \mathbb{R}^{n_s \times 1}$ are the total discharging and charging efficiencies of the storage units, and \mathbf{I}^{n_s} denotes the identity matrix of dimension n_s . The complete *SoE* evolution $\mathbf{E} = [\mathbf{e}(1), \dots, \mathbf{e}(N)]^T$ for a time horizon of length N is

$$\mathbf{E} = \underbrace{\begin{bmatrix} \mathbf{I}^{n_s} \\ \vdots \\ \mathbf{I}^{n_s} \end{bmatrix}}_{\mathbf{S}_x} \mathbf{e}(0) + \underbrace{\begin{bmatrix} \mathbf{B} & \mathbf{0} \\ \vdots & \ddots \\ \mathbf{B} & \cdots & \mathbf{B} \end{bmatrix}}_{\mathbf{S}_u} \underbrace{\begin{bmatrix} \mathbf{p}_{\text{gen}}^{\text{s}}(0) \\ \vdots \\ \mathbf{p}_{\text{gen}}^{\text{s}}(N) \end{bmatrix}}_{\mathbf{U}}, \tag{13}$$

where $\mathbf{e}(0)$ is the initial *SoE* vector.

2) *Incorporation of Battery Degradation:* In Section III-C we calculated the piecewise-affine (PWA) convex hull (10) of the degradation map. To incorporate degradation into the planning problem, we define helper decision variables $\mathbf{Z} = [\mathbf{z}(1), \dots, \mathbf{z}(N) \in \mathbb{R}^{n_s \times 1}]^T$ and include the epigraphs of (10) as constraints in our problem. Specifically, we substitute \mathbf{E}

from (13) into an extended version of (10) that includes n_s battery systems and obtain a degradation equation in terms of the control variable \mathbf{U} as follows:

$$(\mathbf{A}_1 + \mathbf{A}_2 \mathbf{S}_u) \mathbf{U} + \mathbf{A}_z \mathbf{Z} \leq -\mathbf{A}_2 \mathbf{S}_x \mathbf{e}_0 - \mathbf{A}_3 \mathbf{c}_E, \quad (14)$$

where $\mathbf{A}_1 = [\mathbf{I}^{Nn_s} \otimes \mathbf{a}_1] [-\mathbf{I}^{Nn_s} - \mathbf{I}^{Nn_s}]$, $\mathbf{A}_2 = [\mathbf{I}^{Nn_s} \otimes \mathbf{a}_2]$, $\mathbf{A}_3 = [\mathbf{1}^{Nn_s \times 1} \otimes \mathbf{a}_3]$, and $\mathbf{A}_z = [\mathbf{I}^N \otimes -\mathbf{1}^{n_s \times 1}]$. The operator \otimes denotes the Kronecker product.

3) *Robust Scheduling*: To solve a multi-period OPF we first incorporate a temporally-coupled sequence of single period OPF problems (11). We extend the decision vector to $\mathbf{X} = [\mathbf{x}_1, \dots, \mathbf{x}_N]^T$, where $\mathbf{p}_{\text{gen},i} = [p_{\text{net},i} \ \mathbf{p}_{\text{gen},i}^s]^T \in \mathbf{x}_i$ and $p_{\text{net},i}$ (i.e., the net power into or out of the LAC) is treated as a slack generator. Since we do not allow for PV curtailment, we set

$$\mathbf{p}_{d,i} = -\mathbf{C}_{\text{pv}}(\hat{\mathbf{p}}_{\text{gen},i}^{\text{pv}} + \mathbf{w}_i 3\sigma_{\text{pv},i}^T) + \hat{\mathbf{p}}_{\text{ld}}, \quad (15)$$

where the PV and load forecasts are denoted by $\hat{\mathbf{p}}_{\text{gen},i}^{\text{pv}}$ and $\hat{\mathbf{p}}_{\text{ld}}$, and $\mathbf{C}_{\text{pv}} \in \mathbb{R}^{n \times n_{\text{pv}}}$ maps the n_{pv} PV units to the buses. The standard deviation $\sigma_{\text{pv},i}$ of the PV forecast error could be determined by using the results from [25]. We define $\mathbf{W} = [\mathbf{w}_1, \dots, \mathbf{w}_N]^T$, which is a box-constrained uncertainty set where $-1 \leq \mathbf{W} \leq 1$. Note that we do not consider load forecast uncertainty, since absolute load forecast errors are generally much smaller than absolute PV forecast errors for a grid with high PV penetration. The scheduling problem is

$$\begin{aligned} \min_{\mathbf{X}, \mathbf{Z}} \quad & T_1 \left(\sum_{k=0}^N c_n p_{\text{net}}(k) + c_d \mathbf{1}^T \mathbf{z}(k) \right) \\ \text{s.t.} \quad & \text{(a) } -\mathbf{S}_x \mathbf{e}(0) \leq \mathbf{S}_u \mathbf{U} \leq \mathbf{c}_E - \mathbf{S}_x \mathbf{e}(0) \\ & \forall \mathbf{x} : \max_{-1 \leq \mathbf{W} \leq 1} (11\text{a-c,e}), (11\text{d,g-l}), (14), \end{aligned} \quad (16)$$

where c_n and c_d are cost parameters for the net power and the battery degradation. With this formulation, the PV infeed will be maximized since the optimizer minimizes p_{net} . The constraint set (16a) operates the storage devices at their minimum and maximum bounds. To retrieve the robust counterpart of (16), we eliminate \mathbf{w}_i and use $|\sigma_{\text{pv},i}|$ within each constraint [26], since \mathbf{X} does not multiply the random variable [27].

4) *Determination of Robust Storage Level Bounds*: To link the planning domain with the RT domain, the scheduler sends robust allocation bounds for the RT controller

$$\mathbf{e}_{\min} = \min(\mathbf{e}(0), \mathbf{e}(1)) \quad (17)$$

$$\mathbf{e}_{\max} = \max(\mathbf{e}(0), \mathbf{e}(1)), \quad (18)$$

where we evaluate $\mathbf{e}(1)$ with (13). The scheduler also sends the aggregated battery setpoint $p_{\text{bat}}^{\text{agg}}$ to give the RT controller the ability to operate the batteries at their individual optimal operation points

$$\mathbf{p}_{\text{bat}}^{\text{agg}} = \mathbf{1}^T \mathbf{p}_{\text{gen}}^{\text{*s}}(1), \quad (19)$$

where $\mathbf{p}_{\text{gen}}^{\text{*s}}(1)$ is a portion of the optimal decision vector of the robust problem (16).

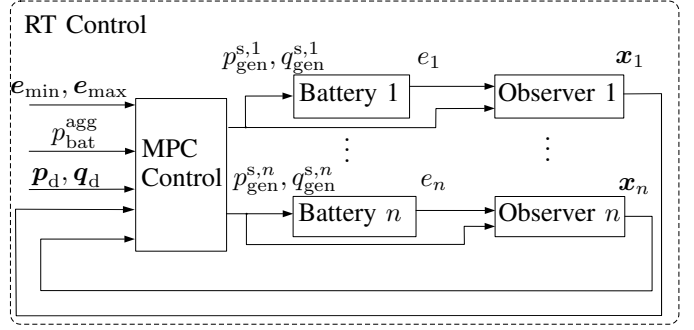


Figure 8. Block diagram of the RT controller.

C. Real-Time Control

As depicted in Fig. 8, the RT controller receives the storage allocation bounds and aggregated battery power setpoint. Using real-time measurements of the PV injections $\mathbf{p}_{\text{gen}}^{\text{pv}}, \mathbf{q}_{\text{gen}}^{\text{pv}}$ and loads $\mathbf{p}_{\text{ld}}, \mathbf{q}_{\text{ld}}$ to compute $\mathbf{p}_d, \mathbf{q}_d$, it sets the reactive and active battery powers $\mathbf{p}_{\text{gen}}^s, \mathbf{q}_{\text{gen}}^s$ by solving an RT-OPF. In particular, we solve an MPC problem for one step incorporating the linear extended battery model (9), allowing us to estimate the power available from each individual battery system and utilize its full capacity potential. The decision vector is $\mathbf{u}_0 = [\mathbf{p}_{\text{gen}}^s \ \mathbf{q}_{\text{gen}}^s \ \lambda \ \mathbf{p}_{\text{bat}}^{\text{loss}} \ y_{\text{set}}^{\text{agg}} \ \mathbf{x}_{\text{set}}]^T$, where λ and $\mathbf{p}_{\text{bat}}^{\text{loss}}$ are helper variables to incorporate battery losses into the problem and $y_{\text{set}}^{\text{agg}}$ and \mathbf{x}_{set} are helper variables to penalize deviations from the storage allocation bounds. The RT-OPF problem is

$$\begin{aligned} \min_{\mathbf{u}_0} \quad & \underbrace{\mathbf{1}^T \mathbf{p}_{\text{gen}}}_{\text{network losses}} + \underbrace{\mathbf{1}^T \mathbf{p}_{\text{bat}}^{\text{loss}}}_{\text{battery losses}} + \underbrace{y_{\text{set}}^{\text{agg}} + \mathbf{1}^T \mathbf{x}_{\text{set}}}_{\text{deviations from setpoint regions}} \\ \text{s.t.} \quad & \text{(11a) - (11l)} \\ & \text{(a) } \mathbf{X}_1 = \Phi \mathbf{X}_0 + \mathbf{H} \mathbf{p}_{\text{gen}}^s \\ & \text{(b) } \mathbf{0} \leq \mathbf{X}_1 \leq \mathbf{1}^{n_s \times 1} \otimes \begin{bmatrix} c_w \\ 1 - c_w \end{bmatrix} \\ & \text{(c) } -\text{diag}\{\mathbf{m}\} \mathbf{C} \mathbf{X}_1 - \mathbf{I}^{n_s} \mathbf{x}_{\text{set}} \leq -\mathbf{e}_{\min} m \\ & \text{(d) } \text{diag}\{\mathbf{m}\} \mathbf{C} \mathbf{X}_1 - \mathbf{I}^{n_s} \mathbf{x}_{\text{set}} \leq \mathbf{e}_{\max} m \\ & \text{(e) } \mathbf{I}^{n_s} \mathbf{x}_{\text{set}} \leq \mathbf{0} \\ & \text{(f) } -m \mathbf{1}^T \mathbf{p}_{\text{gen}}^s - y_{\text{set}}^{\text{agg}} \leq -m p_{\text{bat}}^{\text{agg}} \\ & \text{(g) } -m \mathbf{1}^T \mathbf{p}_{\text{gen}}^s - y_{\text{set}}^{\text{agg}} \leq 0 \\ & \text{(h) } \mathbf{p}_d = -\mathbf{C}_{\text{pv}} \mathbf{p}_{\text{gen}}^{\text{pv}} + \mathbf{p}_{\text{ld}} \\ & \text{(i) } \mathbf{q}_d = -\mathbf{C}_{\text{pv}} \mathbf{q}_{\text{gen}}^{\text{pv}} + \mathbf{q}_{\text{ld}} \\ & \text{(j) } -\mathbf{I}^{n_s} \mathbf{p}_{\text{gen}}^s + [\mathbf{I}^{n_s} \otimes \mathbf{p}_{\text{gen}}^{\text{s,P}}] \lambda = \mathbf{0} \\ & \text{(k) } -\mathbf{I}^{n_s} \mathbf{p}_{\text{bat}}^{\text{loss}} + [\mathbf{I}^{n_s} \otimes f(\mathbf{p}_{\text{gen}}^{\text{s,P}})] \lambda = \mathbf{0} \\ & \text{(l) } [\mathbf{I}^{n_s} \otimes \mathbf{1}^{1 \times n_s}] \lambda = \mathbf{1} \\ & \text{(m) } \lambda = [\lambda_1, \dots, \lambda_{n_s}]^T \ \forall \lambda_i : \text{SOS2}, \end{aligned} \quad (20)$$

where (20a) is the discrete version of (9) for multiple battery systems. Specifically, \mathbf{X}_0 is the initial battery system state and \mathbf{X}_1 is the state after one time step; Φ is the battery system dynamics matrix, \mathbf{H} is the RT control input matrix, and \mathbf{C} maps the internal states of each battery system to the *SoE*. Constraint (20b) avoids overspill of the battery capacity wells. Constraints (20c-e) define two regions and enable us to penalize deviations outside of the storage allocation bounds $\mathbf{e}_{\min}, \mathbf{e}_{\max}$ with the penalty factor m , where $\text{diag}\{\mathbf{m}\}$ is a square matrix with m on the diagonal. We only penalize

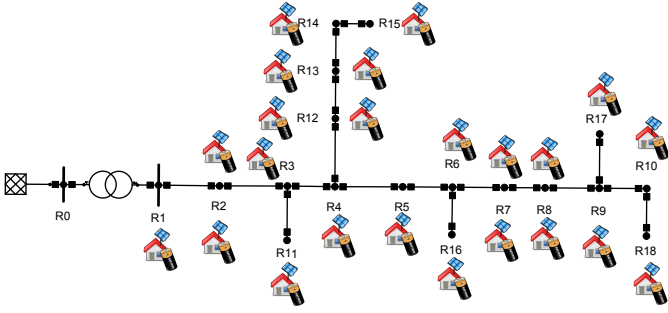


Figure 9. Modified Cigre test grid [24] with PV generators (20kW) and battery storage units (10kVA/20kWh).

the aggregated power setpoint in the discharging direction with (20f,g), since overcharging can be dealt with in RT as it will not result in line limit violations. This yields lower storage utilization and thus results in lower battery degradation. Constraints (20h,i) incorporate the RT measurements and (20j-m) represent nonconvex piecewise linear functions of the battery losses using an efficient Special Ordered Set (SOS) formulation [28]. In particular, we discretize (6) with P supporting points $p_{\text{gen}}^{s,P}$ and evaluate (6) for each point and for each battery system. The sum of the elements in the set λ_i has to be equal to 1, which is enforced in (20l), and at most two elements in the set have to be consecutively non-zero (20m). This is referred to as an SOS2 set. Constraint (20m) makes the problem a Mixed Integer Linear Programming (MILP) problem.

We also implemented an observer to estimate the internal states x_E of each individual battery system, since battery management systems typically provide only the SoE . Since the system (9) is detectable, [29] we can design following Luenberger observer

$$\dot{\hat{x}}_E = (\mathbf{A} - \mathbf{l}[1 \ 1])\hat{x}_E + \begin{bmatrix} 1 & \mathbf{l} \\ 0 & \mathbf{l} \end{bmatrix} \begin{bmatrix} P_{\text{bat}} \\ SoE \end{bmatrix}, \quad (21)$$

where $\mathbf{l} \in \mathbb{R}^{2 \times 1}$ is chosen such that $(\mathbf{A} - \mathbf{l}[1 \ 1])$ is stable.

VI. SIMULATION RESULTS

Through case studies we demonstrate the performance of our centralized control scheme. The parameters are listed in Table I. Figure 9 shows the units within the test grid. We assess each control stage with simulations on different timescales. To study the RT controller, we simulate its performance on a sunny day and use the high-fidelity model DUALFOIL [30] in place of a real battery system. To study the impact of the scheduler on battery lifetimes, we need to consider a long time horizon. However, to reduce simulation times, we omit the RT stage and run our scheduler with the simplified battery model and model the capacity loss with the convexified degradation maps.

A. RT control performance

In Fig. 10 we show the RT evolution of the battery energy levels. The gray boxes are the allocation bounds e_{\min}, e_{\max} from the scheduler. The scheduler uses the linear basic model,

Table I
SIMULATION PARAMETERS.

Storage units	18
Storage parameter	$p_{\text{gen}}^{s,\max} = 10\text{kW}, q_{\text{gen}}^{s,\max} = 10\text{kVar}, c_E = 20\text{kWh}$
Deg. model LiCoO2	convexified degradation map from [9]
Deg. model LiFePO4	convexified degradation map from [21]
Scheduler horizon N	24 @ 1h sample time
Net power cost c_n	100 €/kWh
Degradation cost c_d	400 €/kWh
Supporting points	$P = 10$
Charging Efficiency	0.91
Discharging Efficiency	0.91
PV units	18
PV power	$p_{\text{gen}}^{\text{pv},\max} = 20 \text{ kW } (\lambda = 1)$
Simulation Horizon	1 year
Households	18 @ 4kW (randomized profile)
Grid	European LV network [24]
Voltage Limits	$v_{\max} = 1.1, v_{\min} = 0.9$

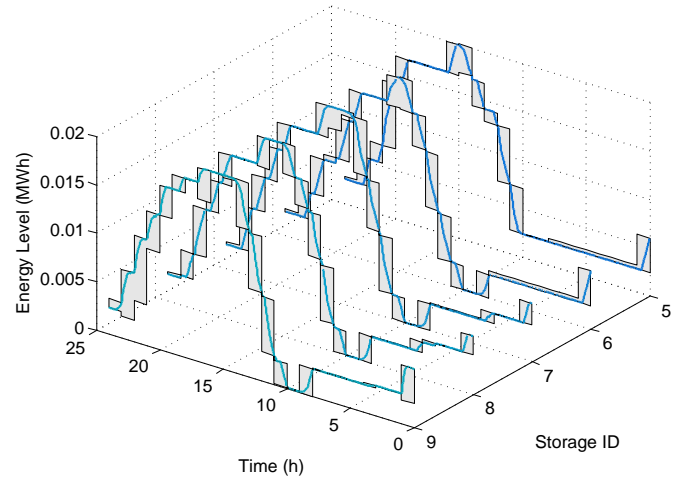


Figure 10. RT evolution of the battery energy levels. The gray boxes are the storage allocation bounds from the scheduler, in which the RT controller can operate. For high state of energy regimes, the RT controller has to reduce the battery power to make the full capacity available.

which does not include the rate capacity effect. However, the RT controller uses the linear extended model and so, in high state of energy regimes, it reduces the battery power to make the full capacity available, corresponding to a slower rise in energy levels.

To reduce battery system losses, the RT controller dispatches the batteries to loss-optimal operating points, while keeping them within the allocation bounds. This can be seen in Fig. 11, where the RT controller sets the battery powers in a rolling fashion, resulting in switched battery operation.

Figure 12 shows compliance with the voltage and line flow constraints. Since we use a linear approximation of the power flow in our controllers, we calculate the exact power flows by running the full nonlinear AC power flow with all power injection variables set to the setpoints calculated by the RT controller. As already shown in [11], the linear approximation leads to a solution that is always feasible. This we can see from Fig. 12, since the maximum line capacity is not fully utilized and the allowable voltage band (0.9 – 1.1 pu) is not fully used.

To illustrate the merit of the detailed power loss model,

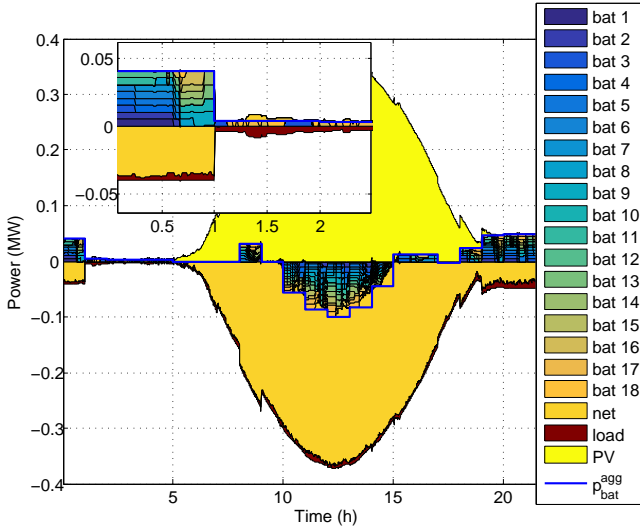


Figure 11. RT dispatch for a one day simulation with a snapshot of the battery discharging phase. The blue curve shows the aggregated battery power signal from the scheduler. To reduce battery losses, the batteries are discharged (positive powers) and charged (negative powers) in a switched way.

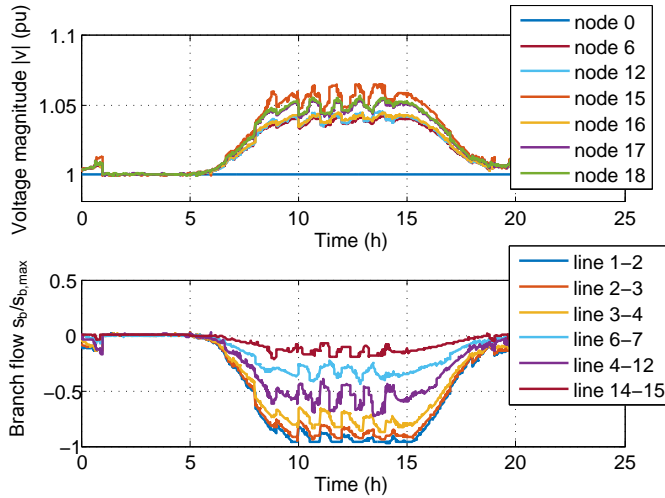


Figure 12. Voltage magnitudes and normalized branch power flows for a one day simulation with high PV infeed. The allowable voltage band is $v_{\min} = 0.9$ to $v_{\max} = 1.1$ pu.

we simulate the RT controller using the full model in (20) (referred to as the RT-MILP configuration) and using a simpler linear loss model, resulting in an LP problem (referred to as the RT-LP configuration). As shown in Fig. 13 the battery losses are 30% smaller, if we use the RT-MILP configuration. Table II quantifies this finding. The loss reduction is mainly due to the reduced battery losses. Network losses are almost identical in both cases and are approximately one third of the network losses.

B. Lifetime Assessment

We next determine how the scheduler affects battery lifetimes, and compare two different battery technologies: LiCoO₂ and LiFePO₄. For LiCoO₂, we take the degradation map from [9]. For LiFePO₄, we discretize the analytic degradation function presented in [21] to obtain a map. Both maps are

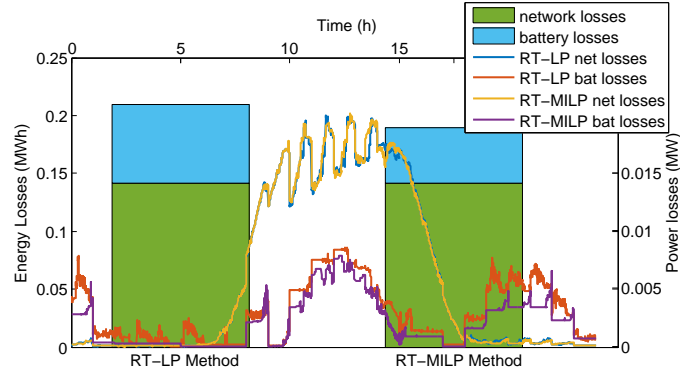


Figure 13. Battery and network losses for a sunny day. The bars show the energy losses as a function of the RT control configuration. The curves show power loss over the day for the different RT control configurations. With the detailed loss model (RT-MILP) the system incurs almost 30% fewer losses.

Table II
LOSSES FOR DIFFERENT RT CONTROL CONFIGURATIONS.

RT control configuration	battery loss model	network losses (kWh)	battery losses (kWh)
RT-MILP	nonconvex	141.8	47.5
RT-LP	linear	141.2	68.4

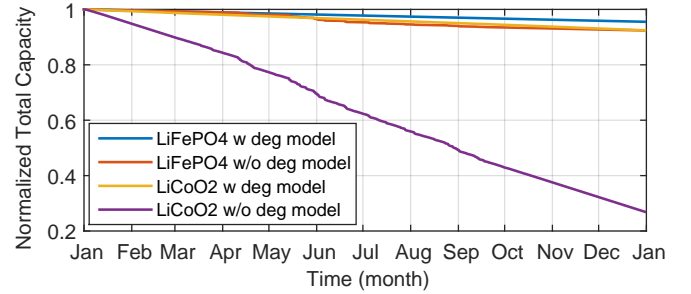


Figure 14. Normalized total battery capacity over one year for different battery technologies, with (w) and without (w/o) a degradation (deg) model.

convexified as described in Section III-C and are included in the scheduler. We also simulate the scheduler without using the degradation model, but constrain the minimum SoE level to 5% of the capacity. In Fig. 14, we compare the charge capacity loss over one year for the different battery technologies. The scheduler without the degradation model operates the batteries in low SoE regimes. Those regimes result in high degradation, especially for the LiCoO₂ system. In Fig. 15, we also show the charge capacity loss for each battery. Using degradation models, the scheduler balances degradation across the batteries, contributing to longer battery lifetimes (see Table III). We also extrapolated these results to obtain estimates for the number of full cycles and lifetimes assuming an end of life (EOL) criterion of 0.8, which means that 80% of the initial capacity remains. We find that by using a degradation model, we can prolong the lifetime by a factor 10 for the LiCoO₂ system and by a factor 2 for the LiFePO₄.

VII. CONCLUSION

In this paper, we present a novel two-stage centralized MPC scheme for distributed battery storage to mitigate voltage and

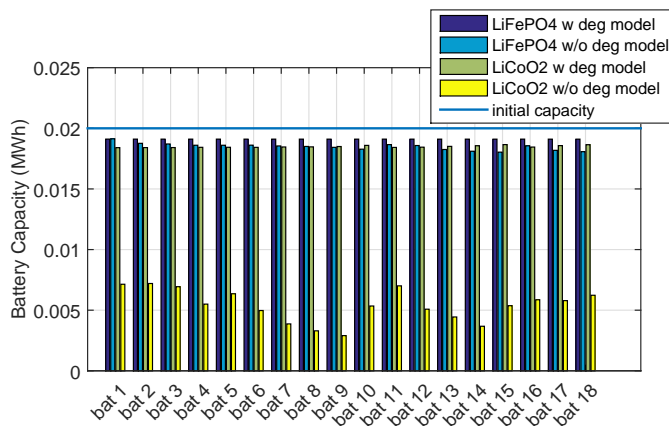


Figure 15. Remaining battery capacities for each battery (bat) after a one year simulation for different battery technologies, with (w) and without (w/o) a degradation (deg) model. The blue line shows the initial battery capacities.

Table III
LIFE TIME ASSESSMENT FOR DIFFERENT BATTERY TECHNOLOGIES.

Battery Technology	Configuration	Expected number of full cycles	Expected lifetime (years)
LiFePO4	w deg model	2816	4.4
	w/o deg model	1609	2.64
LiCoO2	w deg model	1652	2.63
	w/o deg model	166	0.29

line flow violations that are induced by high PV penetrations in LV grids. To link the planning and real time domains, our control scheme consists of a robust scheduler and a RT controller. This division enables planning using course PV and load forecasts on timescales of hours and RT control to manage dynamics and forecast error on timescales of seconds. Therefore, the scheduler uses simple battery models, while the RT controller uses detailed models. We incorporate a linearized AC-OPF into both the scheduler and RT controller to reduce the computational complexity of the algorithms. To guarantee secure grid operation, the scheduler solves a robust multi-period OPF taking the worst-case PV forecast into account. It produces robust feasible storage allocation bounds for the RT controller, which maximizes PV utilization, while keeping battery degradation to a minimum by solving a single step OPF problem. We find that the control scheme can substantially reduce both battery losses and degradation.

REFERENCES

- [1] "Battery energy storage for smart grid applications," Eurobat, Tech. Rep., 2013. [Online]. Available: https://http://www.eurobat.org/sites/default/files/eurobat_smartgrid_publication_may_2013_0.pdf
- [2] F. Marra, G. Yang, C. Træholt, J. Østergaard, and E. Larsen, "A decentralized storage strategy for residential feeders with photovoltaics," *IEEE Transactions on Smart Grid*, vol. 5, no. 2, pp. 974–981, 2014.
- [3] K. H. Chua, Y. S. Lim, P. Taylor, S. Morris, and J. Wong, "Energy storage system for mitigating voltage unbalance on low-voltage networks with photovoltaic systems," *IEEE Transactions on Power Delivery*, vol. 27, no. 4, pp. 1783–1790, 2012.
- [4] T. Wang, H. Kamath, and S. Willard, "Control and optimization of grid-tied photovoltaic storage systems using model predictive control," *IEEE Transactions on Smart Grid*, vol. 5, no. 2, pp. 1010–1017, 2014.
- [5] B. Nykvist and M. n. Nilsson, "Rapidly falling costs of battery packs for electric vehicles," *Nature Climate Change*, vol. 5, no. 4, pp. 329–332, 2015.
- [6] S. J. Moura, J. C. Forman, S. Bashash, J. L. Stein, and H. K. Fathy, "Optimal Control of Film Growth in Lithium-Ion Battery Packs via Relay Switches," *IEEE Transactions on Industrial Electronics*, vol. 58, no. 8, pp. 3555–3566, 2011.
- [7] M. Koller, T. Borsche, A. Ulbig, and G. Andersson, "Defining a degradation cost function for optimal control of a battery energy storage system," in *Proceedings of POWERTECH*, 2013, pp. 1–6.
- [8] A. Trippe, R. Arunachala, T. Massier, J. Jossen, and T. Hamacher, "Charging optimization of battery electric vehicles including cycle battery aging," in *Proceedings of ISGT EUROPE*, Oct 2014.
- [9] P. Fortenbacher, J. Mathieu, and G. Andersson, "Modeling, identification, and optimal control of batteries for power system applications," in *Proceedings of the Power Systems Computation Conference*, 2014.
- [10] —, "Optimal real-time control of multiple battery sets for power system applications," in *Proceedings of POWERTECH*, 2015.
- [11] P. Fortenbacher, M. Zellner, and G. Andersson, "Optimal sizing and placement of distributed storage in low voltage networks," in *accepted for 19th Power Systems Computation Conference, Genoa, Italy*, 2016. [Online]. Available: <http://arxiv.org/abs/1512.01218>
- [12] D. K. Molzahn and I. A. Hiskens, "Moment-Based Relaxation of the Optimal Power Flow Problem," in *Proceedings of Power Systems Computation Conference*, 18–22 Aug. 2014.
- [13] S. H. Low, "Convex relaxation of optimal power flow - part I: Formulations and equivalence," *IEEE Transactions on Control of Network Systems*, vol. 1, no. 1, pp. 15–27, March 2014.
- [14] K. Christakou, D.-C. Tomozei, J.-Y. L. Boudec, and M. Paolone, "AC OPF in Radial Distribution Networks - Parts I,II," 2015. [Online]. Available: <http://arxiv.org/abs/1503.06809>
- [15] R. Tonkoski, L. A. Lopes, and T. H. El-Fouly, "Coordinated active power curtailment of grid connected pv inverters for overvoltage prevention," *IEEE Trans on Sustainable Energy*, vol. 2, no. 2, pp. 139–147, 2011.
- [16] G. Kerber, R. Witzmann, and H. Sappl, "Voltage limitation by autonomous reactive power control of grid connected photovoltaic inverters," in *Compatibility and Power Electronics*, May 2009, pp. 129–133.
- [17] "VDE-AR-N 4105 power generation systems connected to the low-voltage distribution network - technical minimum requirements for the connection to and parallel operation with low-voltage distribution networks," *VDE Application Rule*, 2011.
- [18] "Efficiency and derating sunny boy / sunny tripower / sunny mini central," SMA, Tech. Rep., 2015. [Online]. Available: <http://files.sma.de/dl/1348/WirkungDerat-TI-en-40.pdf>
- [19] M. Doyle and J. Newman, "Analysis of capacity-rate data for lithium batteries using simplified models of the discharge process," *Journal of Applied Electrochemistry*, vol. 27, no. 7, pp. 846–856, 1997.
- [20] J. F. Manwell and J. G. McGowan, "Lead acid battery storage model for hybrid energy systems," *Solar Energy*, vol. 50, no. 5, pp. 399 – 405, 1993.
- [21] J. C. Forman, S. J. Moura, J. L. Stein, and H. K. Fathy, "Optimal Experimental Design for Modeling Battery Degradation," in *Proceedings of ASME Dynamic Systems and Control Conference*, vol. 1, 2012, pp. 309–318.
- [22] D. T. Lee and B. J. Schachter, "Two algorithms for constructing a delaunay triangulation," *International Journal of Computer & Information Sciences*, vol. 9, no. 3, pp. 219–242.
- [23] J.-H. Teng, "A direct approach for distribution system load flow solutions," *IEEE Transactions on Power Delivery*, vol. 18, no. 3, pp. 882–887, July 2003.
- [24] "Benchmark systems for network integration of renewable and distributed energy resources," Cigre Task Force C6.04.02, Tech. Rep., 2014. [Online]. Available: <http://c6.cigre.org/Publications/Technical-Brochures>
- [25] P. Bacher, H. Madsen, and H. A. Nielsen, "Online short-term solar power forecasting," *Solar Energy*, vol. 83, no. 10, pp. 1772 – 1783, 2009.
- [26] A. Ben-Tal, L. El Ghaoui, and A. Nemirovski, *Robust Optimization*. Princeton University Press, 2009.
- [27] J. Löfberg, "Automatic robust convex programming," *Optimization Methods and Software*, vol. 27, no. 1, pp. 115–129, 2012.
- [28] J. A. Tomlin, "Special ordered sets and an application to gas supply operations planning," *Mathematical Programming*, vol. 42, no. 1, pp. 69–84.
- [29] J. O'Reilly, *Observers for Linear Systems*. Elsevier Science, 1983.
- [30] M. Doyle, T. F. Fuller, and J. Newman, "Modeling of galvanostatic charge and discharge of the lithium/polymer/insertion cell," *Journal of The Electrochemical Society*, vol. 140, no. 6, pp. 1526–1533, 1993.